A Reliable Uplink Control Channel Design with Complementary Sequences

Alphan Şahin, *Member, IEEE,* and Rui Yang, *Member, IEEE*

arXiv:1904.01181v1 [cs.IT] 2 Apr 2019

***Abstract*—In this study, we propose two schemes for uplink control channels based on non-contiguous complementary sequences (CSs) where the peak-to-average-power ratio (PAPR) of the resulting orthogonal frequency division multiplexing (OFDM) signal is always less than or equal to 3 dB. To obtain the proposed schemes, we extend Golay's concatenation and interleaving methods by considering extra upsampling and shifting parameters. The proposed schemes enable a flexible non-contiguous resource allocation in frequency, e.g., an arbitrary number of null symbols between the occupied resource blocks (RBs). The first scheme separates the PAPR minimization and the inter-cell interference minimization problems. While the former is solved by spreading the sequences in a Golay complementary pair (GCP) with the sequences in another GCP, the latter is managed by designing a set of GCPs with low cross-correlation. The second scheme generates reference symbols (RSs) and data symbols on each RB as parts of an encoded CS. Therefore, it enables coherent detection at the receiver side. The numerical results show that the proposed schemes offer significantly improved PAPR and cubic metric (CM) results in case of non-contiguous resource allocation as compared to the sequences defined in 3GPP New Radio (NR) and Zadoff-Chu (ZC) sequences.**

***Index Terms*—Control channels, cubic metric, complementary sequences, PAPR, OFDM, unlicensed spectrum**

I. Introduction

Non-contiguous resource allocation in the frequency domain is a well-known method to enhance the reliability of a link via frequency diversity gain. However, it is often demoted or left as an optional feature as it can cause inter-modulation distortion (IMD) products located outside of the bandwidth; and therefore may violate the emission requirements. On the other hand, for unlicensed bands, non-contiguous resource allocation is considered as a baseline in today's major standards such as 3GPP Long-Term Evolution (LTE) enhanced licensed-assisted access (eLAA), MulteFire, and 3GPP NR-Unlicensed (NR-U). The main reason behind the non-contiguous resource allocation is that it enables multiple accessing in the uplink while allowing a radio to increase the transmit power under stringent power spectral density (PSD) and occupied channel bandwidth (OCB) requirements imposed by the regulatory agencies. For example, based on ETSI regulations [1], the PSD of the transmitted signal should be less than 10 dBm/Mhz while the OCB should be larger than 80% of the nominal channel bandwidth in the 5 GHz band. Therefore, the maximum transmit power of an uplink signal which consists of only a single resource block (RB) (e.g., 180 kHz in LTE), will be limited to 10 dBm and the narrow bandwidth transmission will violate the regulations due to the OCB requirement. To be able to increase the transmit power under the PSD constraint, while complying with the OCB requirement, non-contiguous resource allocation is adopted in LTE eLAA uplink, which is a major difference as compared to the one for legacy LTE. The basic unit of the resource allocation for LTE eLAA data channels is defined as an *interlace* which is composed of 10 equally-spaced RBs within a 20 MHz bandwidth. A similar non-contiguous allocation, but more flexible in terms of bandwidth and subcarrier spacing, is also expected to be considered in NR-U.

The instantaneous peak power of orthogonal frequency division multiplexing (OFDM) signal with arbitrary information symbols in frequency can be high, which can degrade the transmission power efficiency and decrease the coverage range of a link due to the power back-off. Non-contiguous resource allocation introduces an additional challenging constraint on peak-to-average-power ratio (PAPR) minimization. This issue can also be a detrimental factor for the reliability, particularly when transmitting very short packet with one or two OFDM symbols for latency reduction. In this study, we address the issue of the high instantaneous peak power of an OFDM symbol with a non-contiguous resource allocation and consider the cases where the transmitter needs to transmit a small amount of information such as ACK/NACK or scheduling request (SR) in the uplink.

In the literature, there are many approaches investigating PAPR minimization for OFDM [2]. For example, with partial transmit sequences (PTS) [3], additional phase rotations are applied to the symbol groups in frequency such that the resulting signal has low PAPR. However, PTS can increase the overhead as the receiver may need to know the rotations. Companding transform is another widely-used method which compensates the distortion from hardware non-linearity at the expense of higher bit-error rate (BER) [4]. Another approach is discrete Fourier transform (DFT) precoding [5], i.e., DFT-spread OFDM, where the multicarrier structure of a plain OFDM symbol is effectively converted to a wideband single carrier waveform [6]. It substantially decreases the fluctuations in time when the resource allocation is contiguous in the frequency and low-order modulation symbols are utilized. It also allows several methods such as frequency domain windowing to decrease the PAPR further [7]. On the other hand, in cases of non-contiguous resource allocation after DFT precoding, the low-PAPR benefit of DFT-spread OFDM diminishes as it loses its single carrier structure. The approaches that take the encoding into account for reducing PAPR may require a joint design that typically imposes additional constraints on

Alphan Şahin and Rui Yang are affiliated with InterDigital, Huntington Quadrangle, Melville, NY. email: {alphan.sahin, rui.yang}@interdigital.com

coding structure, modulation type, and waveform parameters such as resource allocation. For example, by exhaustive search for parity bits that lead to low PAPR [8] or by using offsets from linear code [9] are several methods that place constraints on the parity bits. In [10], Daoud and Alani proposed to use low-density parity check (LDPC) codes to mitigate the PAPR of OFDM symbols via exhaustive search. In [11], various interleavers were proposed for Turbo encoder to reduce PAPR. To mitigate PAPR via encoding, a remarkable method has been established with complementary sequences (CSs) [12], especially after the connection between CSs and Reed-Muller codes was discovered by Davis and Jedwab [13]. However, synthesizing CSs for a given resource allocation is still a challenging task. Recently, a theoretical framework was proposed to synthesize a CS with null symbols, i.e., non-contiguous CS [14]. Nevertheless, the practical applications of non-contiguous CSs are still in their early stage.

In this study, we propose two schemes for the uplink control channel where the PAPR of the resulting OFDM symbol is restricted below a certain level by exploiting the non-contiguous CSs obtained via Theorem 1 given in Section III. The first scheme enables non-coherent detection at the receiver while mitigating the interference from other cells in the network with well-designed CSs that restrict the PAPR to be less than or equal to 3 dB. This scheme can be considered as an extension of the uplink control channel Format 0 in 3GPP New Radio (NR) developed for licensed bands [15]. The second scheme exploits the properties of Theorem 1 and yields an OFDM symbol which includes built-in reference symbols as part of encoded CS. Therefore, it enables coherent detection at the receiver side.

The rest of the paper is organized as follows. In Section II, we provide preliminary discussions on the polynomial representation of sequences and Golay complementary pairs (GCPs). In Section III, we provide Theorem 1 and discuss the proposed schemes. In Section IV, we present numerical results and compare them with other potential approaches. We conclude the paper in Section V.

Notation: The field of complex numbers, the set of integers, and the set of positive integers are denoted by $\mathbb{C}$, $\mathbb{Z}$, and $\mathbb{Z}^+$, respectively. The symbols i, j, $+$, and $-$ denote $\sqrt{-1}$, $-\sqrt{-1}$, 1, and -1, respectively. A sequence of length N is represented by $\boldsymbol{a} = (a_0, a_1, \ldots, a_{N-1})$. The element-wise complex conjugation and the element-wise absolute operation are denoted by $(\cdot)^*$ and $|\cdot|$, respectively. The operator $\tilde{\boldsymbol{a}}$ reverses the order of the elements of $\boldsymbol{a}$ and applies element-wise complex conjugation. The operation $\uparrow_k \{\boldsymbol{a}\}$ introduces $k-1$ null symbols between the elements of $\boldsymbol{a}$. The operations $\boldsymbol{a} \pm \boldsymbol{b}$, $\boldsymbol{a} \odot \boldsymbol{b}$, $\boldsymbol{a} * \boldsymbol{b}$, and $\langle \boldsymbol{a}, \boldsymbol{b} \rangle$ are the element-wise summation/subtraction, the element-wise multiplication, linear convolution, and the inner product of $\boldsymbol{a}$ and $\boldsymbol{b}$, respectively.

II. Preliminaries and Further Notation

A. Polynomial Representation of a Sequence

The polynomial representation of the sequence $\boldsymbol{a}$ can be given by

$$p_{\boldsymbol{a}}(z) \triangleq a_{N-1} z^{N-1} + a_{N-2} z^{N-2} + \cdots + a_0 \ , \qquad (1)$$

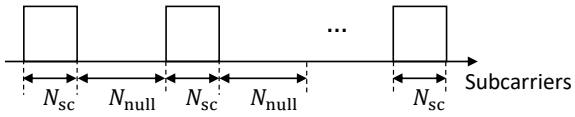


Figure 1. Interlace model.

where $z \in \mathbb{C}$ is a complex number. One can show that the polynomial $p_{\boldsymbol{a}}(z^k)$, $p_{\boldsymbol{a}}(z^k)p_{\boldsymbol{b}}(z^l)$, and $p_{\boldsymbol{a}}(z)z^m$ represent the up-sampled sequence $\boldsymbol{a}$ with the factor of $k \in \mathbb{Z}^+$, the convolution of the up-sampled sequence $\boldsymbol{a}$ with the factor of k and the up-sampled sequence $\boldsymbol{b}$ with the factor of $l \in \mathbb{Z}^+$, and the sequence $\boldsymbol{a}$ padded with $m \in \mathbb{Z}^+$ null symbols, respectively. In addition, by restricting z to be on the unit circle in the complex plane, i.e., $z \in \{\mathrm{e}^{\mathrm{i}\frac{2\pi t}{T_{\text{s}}}} | 0 \le t < T_{\text{s}}\}$, the polynomial representation given in (1) corresponds to an OFDM symbol in continuous time where the elements of the sequence $\boldsymbol{a}$ are mapped to the subcarriers with the same order and T_{s} denotes the OFDM symbol duration.

B. Golay Complementary Pair and Complementary Sequence

The sequence pair $(\boldsymbol{a}, \boldsymbol{b})$ of length N is called a GCP if

$$\rho_{\boldsymbol{a}}(k) + \rho_{\boldsymbol{b}}(k) = 0, \quad \text{for } k \neq 0 \qquad (2)$$

where $\rho_{\boldsymbol{a}}(k)$ is the aperiodic auto correlation (APAC) of the sequence $\boldsymbol{a}$ given by

$$\rho_{\boldsymbol{a}}(k) \triangleq \begin{cases} \rho_{\boldsymbol{a}}^+(k), & \text{if } k \ge 0 \\ \rho_{\boldsymbol{a}}^+(-k)^*, & \text{if } k < 0 \end{cases},$$

and $\rho_{\boldsymbol{a}}^+(k) = \sum_{i=0}^{N-k-1} a_i^* a_{i+k}$ for $k = 0, 1, \ldots, N-1$ and 0 otherwise. The sequences $\boldsymbol{a}$ and $\boldsymbol{b}$ are defined as CSs. By using the definition of GCP, one can show that the GCP $(\boldsymbol{a}, \boldsymbol{b})$ satisfies

$$p_{\boldsymbol{a}}(z)p_{\boldsymbol{a}^*}(z^{-1}) + p_{\boldsymbol{b}}(z)p_{\boldsymbol{b}^*}(z^{-1}) = \rho_{\boldsymbol{a}}(0) + \rho_{\boldsymbol{b}}(0) \ . \qquad (3)$$

By restricting z to be on the unit circle as a further condition, (3) can be written as

$$|p_{\boldsymbol{a}}(z)|^2 + |p_{\boldsymbol{b}}(z)|^2 \Big|_{z=\mathrm{e}^{\mathrm{i}\frac{2\pi t}{T_{\text{s}}}}} = \underbrace{\rho_{\boldsymbol{a}}(0) + \rho_{\boldsymbol{b}}(0)}_{\text{constant}} \ . \qquad (4)$$

The main property that we inherited from GCPs in this study is that the instantaneous peak power of the corresponding OFDM signal generated through a CS $\boldsymbol{a}$ is bounded, i.e., $\max |p_{\boldsymbol{a}}(z)|^2 \le \rho_{\boldsymbol{a}}(0) + \rho_{\boldsymbol{b}}(0)$. Therefore, based on (4), the PAPR of the OFDM signal is less than or equal to $10\log_{10}(2) \approx 3$ dB if $\rho_{\boldsymbol{a}}(0) = \rho_{\boldsymbol{b}}(0)$ [16]. For the other interesting properties of GCPs, we refer the reader to an excellent survey given in [17].

III. Complementary Sequence-Based Interlace Design

We model an interlace as a non-contiguous resource allocation which consists of N_{rb} RBs each of which composed of N_{sc} subcarriers where the RBs are separated by N_{null} tones in the frequency domain as shown in Figure 1. Based on this interlace model, we consider two schemes where the first

one primarily targets non-coherent detectors at receiver and the second scheme enables coherent detectors by yielding to reference symbols (RSs) in each RB. To explain the origin of the proposed schemes, we first restate the following theorem which generalizes Golay's concatenation and interleaving methods [12], [17]:

Theorem 1. *Let $(\boldsymbol{a},\boldsymbol{b})$ and $(\boldsymbol{c},\boldsymbol{d})$ be GCPs of length N and M, respectively, and $\omega_1,\omega_2 \in \{u : u \in \mathbb{C}, |u| = 1\}$ and $k,l,m \in \mathbb{Z}$. Then, the sequences $\boldsymbol{f}$ and $\boldsymbol{g}$ where their polynomial representations given by*

$$p_{\boldsymbol{f}}(z) = \omega_1 p_{\boldsymbol{a}}(z^k)p_{\boldsymbol{c}}(z^l) + \omega_2 p_{\boldsymbol{b}}(z^k)p_{\boldsymbol{d}}(z^l)z^m \ , \quad (5)$$

$$p_{\boldsymbol{g}}(z) = \omega_1 p_{\boldsymbol{a}}(z^k)p_{\tilde{\boldsymbol{d}}}(z^l) - \omega_2 p_{\boldsymbol{b}}(z^k)p_{\tilde{\boldsymbol{c}}}(z^l)z^m \ , \quad (6)$$

construct a GCP.

Proof. Since the sequence pairs $(\boldsymbol{a},\boldsymbol{b})$ and $(\boldsymbol{c},\boldsymbol{d})$ are GCPs, by the definition, $|p_{\boldsymbol{a}}(z)|^2 + |p_{\boldsymbol{b}}(z)|^2 = C_1$ and $|p_{\boldsymbol{c}}(z)|^2 + |p_{\boldsymbol{d}}(z)|^2 = C_2$, where C_1 and C_2 are some constants. To prove that the sequences $\boldsymbol{f}$ and $\boldsymbol{g}$ generated through (5) and (6) construct a GCP, we need to show that $|p_{\boldsymbol{f}}(z)|^2 + |p_{\boldsymbol{g}}(z)|^2$ is also a constant. By exploiting the fact the polynomial representation of the sequence $\tilde{\boldsymbol{a}}$ can be calculated as $p_{\tilde{\boldsymbol{a}}}(z^k) = p_{\boldsymbol{a}^*}(z^{-k})z^{kN-k}$, one can calculate $|p_{\boldsymbol{f}}(z)|^2 + |p_{\boldsymbol{g}}(z)|^2$ as

$$\begin{aligned}
&|p_{\boldsymbol{f}}(z)|^2 + |p_{\boldsymbol{g}}(z)|^2 \\
&= (\omega_1 p_{\boldsymbol{a}}(z^k)p_{\boldsymbol{c}}(z^l) + \omega_2 p_{\boldsymbol{b}}(z^k)p_{\boldsymbol{d}}(z^l)z^m) \\
&\quad \times (\omega_1^* p_{\boldsymbol{a}^*}(z^{-k})p_{\boldsymbol{c}^*}(z^{-l}) + \omega_2^* p_{\boldsymbol{b}^*}(z^{-k})p_{\boldsymbol{d}^*}(z^{-l})z^{-m}) \\
&\quad + (\omega_1 p_{\boldsymbol{a}}(z^k)p_{\tilde{\boldsymbol{d}}}(z^l) - \omega_2 p_{\boldsymbol{b}}(z^k)p_{\tilde{\boldsymbol{c}}}(z^l)z^m) \\
&\quad \times (\omega_1^* p_{\boldsymbol{a}^*}(z^{-k})p_{\tilde{\boldsymbol{d}}^*}(z^{-l}) - \omega_2^* p_{\boldsymbol{b}^*}(z^k)p_{\tilde{\boldsymbol{c}}^*}(z^{-l})z^{-m}) \\
&\overset{(a)}{=} p_{\boldsymbol{a}}(z^k)p_{\boldsymbol{a}^*}(z^{-k})p_{\boldsymbol{c}}(z^l)p_{\boldsymbol{c}^*}(z^{-l}) \\
&\quad + p_{\boldsymbol{a}}(z^k)p_{\boldsymbol{a}^*}(z^{-k})p_{\tilde{\boldsymbol{d}}}(z^l)p_{\tilde{\boldsymbol{d}}^*}(z^{-l}) \\
&\quad + p_{\boldsymbol{b}}(z^k)p_{\boldsymbol{b}^*}(z^{-k})p_{\tilde{\boldsymbol{c}}}(z^l)p_{\tilde{\boldsymbol{c}}^*}(z^{-l}) \\
&\quad + p_{\boldsymbol{b}}(z^k)p_{\boldsymbol{b}^*}(z^{-k})p_{\boldsymbol{d}}(z^l)p_{\boldsymbol{d}^*}(z^{-l}) \\
&\overset{(b)}{=} (p_{\boldsymbol{a}}(z^k)p_{\boldsymbol{a}^*}(z^{-k}) + p_{\boldsymbol{b}}(z^k)p_{\boldsymbol{b}^*}(z^{-k})) \\
&\quad \times (p_{\boldsymbol{c}}(z^l)p_{\boldsymbol{c}^*}(z^{-l}) + p_{\boldsymbol{d}}(z^l)p_{\boldsymbol{d}^*}(z^{-l})) \\
&\overset{(c)}{=} C_1 C_2 \qquad (7)
\end{aligned}$$

where (a) follows from $p_{\tilde{\boldsymbol{c}}^*}(z^{-l})p_{\tilde{\boldsymbol{d}}}(z^l) = p_{\boldsymbol{c}}(z^l)p_{\boldsymbol{d}^*}(z^{-l})$ and $p_{\tilde{\boldsymbol{c}}}(z^l)p_{\tilde{\boldsymbol{d}}^*}(z^{-l}) = p_{\boldsymbol{c}^*}(z^{-l})p_{\boldsymbol{d}}(z^l)$, (b) is because $p_{\tilde{\boldsymbol{c}}}(z^l)p_{\tilde{\boldsymbol{c}}^*}(z^{-l}) = p_{\boldsymbol{c}^*}(z^{-l})p_{\boldsymbol{c}}(z^l)$ and $p_{\tilde{\boldsymbol{d}}}(z^l)p_{\tilde{\boldsymbol{d}}^*}(z^{-l}) = p_{\boldsymbol{d}^*}(z^{-l})p_{\boldsymbol{d}}(z^l)$ and (c) is because of the definition of a GCP. □

Theorem 1 is practically appealing since it can generate CSs with null symbols through the careful choice of the parameters m, k, and l by starting from two GCPs. Therefore, it can be utilized for generating sequences for a non-contiguous resource allocation. In the following subsections, we use the relationships given in Section II-A for the polynomials and exploit Theorem 1 to construct an interlace with the desired resource allocation in the frequency domain.

A. Non-coherent Scheme

In this scheme, we consider a unimodular sequence, i.e., a sequence where the amplitude of each element is 1, for each RB in an interlace. Unimodular sequences are suitable for an uplink control channel since certain cyclic-shifts of an OFDM signal generated through a unimodular sequence are orthogonal to each other [18], which enables code-domain multiple access. Let $\boldsymbol{x} = (x_0, x_1, \ldots, x_{N_{\mathrm{sc}}-1})$ be a unimodular base sequence, i.e., $|x_i| = 1$ for $i \in 0, 1, , \ldots, N_{\mathrm{sc}} - 1$. Then, by representing the cyclic-shift in time domain as modulation in frequency domain,

$$\langle \boldsymbol{y}_{s_1}, \boldsymbol{y}_{s_2} \rangle = 0 \text{ if } s_1 \neq s_2 \ , \quad (8)$$

where

$$\boldsymbol{y}_s = \boldsymbol{x} \odot \boldsymbol{s} \quad (9)$$

for $\boldsymbol{s} = (\xi^{0\times s}, \xi^{1\times s}, \ldots, \xi^{(N_{\mathrm{sc}}-1)\times s})$, $\xi = \mathrm{e}^{\mathrm{i}\frac{2\pi}{N_{\mathrm{sc}}}}$ and $s_1, s_2, s \in \mathbb{Z}$. When unimodular sequences are employed on each RB, the number of orthogonal resources generated through cyclic-shifts in time is limited to the size of RBs. For example, if there are $N_{\mathrm{rb}} = 10$ RBs in one interlace and each RB consists of $N_{\mathrm{sc}} = 12$ subcarriers, there are 12 orthogonal resources generated through the shifts in *time*. 12 resources can be shared by 6 users to transmit 1-bit information (e.g., ACK/NACK) or 3 users to transmit 2-bit information (e.g., ACK/NACK and scheduling request). The receiver can detect the corresponding sequences in each RB non-coherently to decode the information.

To construct the interlace with the proposed scheme, we first choose a GCP $(\boldsymbol{a},\boldsymbol{b})$ of length $N_{\mathrm{rb}}/2$ and a GCP $(\boldsymbol{c}_i,\boldsymbol{d}_i)$ of length N_{sc} where the elements of $\boldsymbol{a}$, $\boldsymbol{b}$, $\boldsymbol{c}_i$ and $\boldsymbol{d}_i$ are in the set $Q_1 \triangleq \{+,-,\mathrm{i},\mathrm{j}\}$ for $i = 1, 2, \ldots, K$ where $K \in \mathbb{Z}^+$. We then generate the interlace through (5) in Theorem 1 by setting $\boldsymbol{c} = \boldsymbol{c}_i$, $\boldsymbol{d} = \boldsymbol{d}_i$, $\omega_1 = \omega_2 = \mathrm{e}^{\frac{\mathrm{i}\pi}{4}}$, $k = N_{\mathrm{sc}} + N_{\mathrm{null}}$, $l = 1$, and $m = (N_{\mathrm{sc}} + N_{\mathrm{null}}) \times N_{\mathrm{rb}}/2$.

In this scheme, $\boldsymbol{a}$ and $\boldsymbol{b}$ act as spreading sequences for the sequences $\boldsymbol{c}_i$ and $\boldsymbol{d}_i$, respectively, since

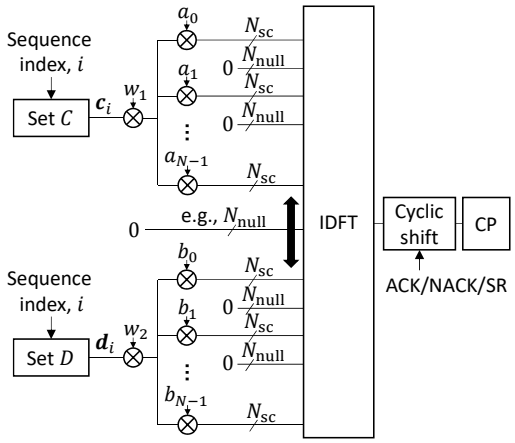
$$p_{\boldsymbol{a}}(z^{N_{\mathrm{sc}}+N_{\mathrm{null}}})p_{\boldsymbol{c}}(z) = p_{\uparrow_{N_{\mathrm{sc}}+N_{\mathrm{null}}}\{\boldsymbol{a}\}*\boldsymbol{c}}(z), \quad (10)$$

and

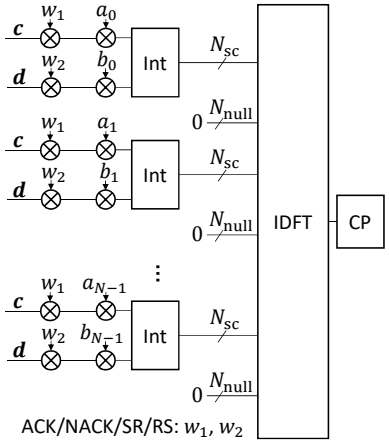
$$p_{\boldsymbol{b}}(z^{N_{\mathrm{sc}}+N_{\mathrm{null}}})p_{\boldsymbol{d}}(z) = p_{\uparrow_{N_{\mathrm{sc}}+N_{\mathrm{null}}}\{\boldsymbol{b}\}*\boldsymbol{d}}(z). \quad (11)$$

In other words, the RBs are constructed with phase rotated versions of $\boldsymbol{c}_i$ and $\boldsymbol{d}_i$ and the phase rotations are determined by the elements of $\boldsymbol{a}$ and $\boldsymbol{b}$ as shown in Figure 2(a). Based on the second part of (5) in Theorem 1, $m = (N_{\mathrm{sc}} + N_{\mathrm{null}}) \times N_{\mathrm{rb}}/2$ null symbols are prepended to the sequence $\uparrow_{N_{\mathrm{sc}}+N_{\mathrm{null}}} \{\boldsymbol{b}\} * \boldsymbol{d}_i$. Hence, while the first half of the interlace is a function of $\boldsymbol{a}$ and $\boldsymbol{c}_i$, the second half of the interlace is generated through $\boldsymbol{b}$ and $\boldsymbol{d}_i$ as illustrated in Figure 2(a). By considering the interlace structure in LTE eLAA, i.e., $N_{\mathrm{sc}} = 12$, $N_{\mathrm{rb}} = 10$, $N_{\mathrm{null}} = 9 \times 12 = 108$ subcarriers, and quadrature phase shift keying (QPSK) alphabet for the sequences, the interlace can be constructed with the proposed scheme via (5) when $k = 120$, $l = 1$, and $m = 600$ and the sequences $\boldsymbol{a}$, $\boldsymbol{b}$, $\boldsymbol{c}_i$, $\boldsymbol{d}_i$ are chosen arbitrarily from the set provided from [19] as $\boldsymbol{a} = (+,+,+,\mathrm{j},\mathrm{i})$, $\boldsymbol{b} = (+,\mathrm{i},-,+,\mathrm{j})$, $\boldsymbol{c}_i = (+,+,+,+,-,-,-,+,\mathrm{i},\mathrm{j},-,+)$, and $\boldsymbol{d}_i = (+,+,\mathrm{i},\mathrm{i},+,+,-,+,+,-,+,-)$.

The proposed scheme offers flexibility for the interlace structure since N_{null} and m can be arbitrary values. For



(a) Transmitter structure for non-coherent scheme.



(b) Transmitter structure for coherent scheme.

Figure 2. Proposed transmitter structures based on CSs

example, in one scenario, another user in the cell may need to transmit a random access signal by using a contiguous allocation[1]. To address this scenario, using a larger m and a *single* pair of shorter spreading sequences $\boldsymbol{a}$ and $\boldsymbol{b}$ can generate the desired gap in the frequency; and the PAPR is still less than or equal to 3 dB for the same $\boldsymbol{c}_i$ and $\boldsymbol{d}_i$. A quick investigation also suggests that the interlace where $\boldsymbol{c}_i$ and $\boldsymbol{d}_i$ are on the adjacent RBs can be constructed when $k = 2(N_{\rm sc} + N_{\rm null})$, $l = 1$, and $m = N_{\rm sc} + N_{\rm null}$, which is another design option offered by the proposed scheme. In this case, the interlace with LTE parameters can be obtained for $k = 240$, $l = 1$, and $m = 120$.

The proposed schemes simplify the control channel design as it separates two complicated problems, i.e., the PAPR minimization for non-contiguous allocation and inter-cell interference minimization. For the first problem, as long as the sequences $\boldsymbol{c}_i$ and $\boldsymbol{d}_i$ for $i = 1, 2, \ldots, K$ construct a GCP, the same spreading $\boldsymbol{a}$ and $\boldsymbol{b}$ can be utilized to limit the PAPR. Note that NR-U may be configured with multiple subcarrier spacing options, e.g., 15, 30, or 60 KHz, and bandwidth, e.g., 20, 40, or 80 MHz. For different configurations, a single GCP is able to limit PAPR to less than or equal to 3 dB for all of the sequences in $C \triangleq \{\boldsymbol{c}_1, \boldsymbol{c}_2, \ldots, \boldsymbol{c}_K\}$ and $D \triangleq \{\boldsymbol{d}_1, \boldsymbol{d}_2, \ldots, \boldsymbol{d}_K\}$, which remarkably reduces the design complexity. For the second problem, the cross-correlation between the sequences used at different cells, i.e., $\boldsymbol{c}_i$ and $\boldsymbol{c}_j$ for $i \neq j$ (and $\boldsymbol{d}_i$ and $\boldsymbol{d}_j$), should be as low as possible to minimize the potential interference among the different cells. Due to the imperfect timing alignment between the uplink signals and the multipath channel, the signal may also be exposed to additional shift in time within the cyclic prefix (CP). In this case, the cross-correlation between the sequences in the sets should consider not only integer shifts, but also non-integer s values in (9). In NR and LTE, the number of available base sequences is set to $K = 30$ for $N_{\rm sc} = 12$. However, designing C and D with a small peak cross-correlation value β, i.e., $\langle \boldsymbol{c}_i, \boldsymbol{c}_j \odot \boldsymbol{s} \rangle \leq \beta$ and $\langle \boldsymbol{d}_i, \boldsymbol{d}_j \odot \boldsymbol{s} \rangle \leq \beta$ for $i \neq j$ and $i, j \in \{1, 2, \ldots, K\}$ and $s \in [0, N_{\rm sc} - 1]$ is challenging task. Therefore, re-using the sets for different configurations is highly desirable. This naturally leads to the following question for the proposed scheme: *Are there any C and D for $K = 30$ and $N_{\rm sc} = 12$, i.e., 30 different GCPs of length 12, such that the peak cross-correlation between any two sequences in each set for any non-integer s value that is sufficiently small?*

To answer this question, we consider a procedure which exploits computer-generated GCPs provided in [19] for length 12 to obtain C and D. We initialize the algorithm with $I = 52$ GCPs of length 12 listed in [19] and populate as $S''_c = \{\boldsymbol{c}''_1, \ldots, \boldsymbol{c}''_I\}$ and $S''_d = \{\boldsymbol{d}''_1, \ldots, \boldsymbol{d}''_I\}$. For the ith seed GCP $(\boldsymbol{c}''_i, \boldsymbol{d}''_i)$, we first enumerate $J = 8$ equivalent GCPs by interchanging, reflecting both (i.e., reversing the order of the elements of the sequences), and conjugate reflecting original sequences in the seed GCP, which lead to the sets $S'_c = \{\boldsymbol{c}'_1, \ldots, \boldsymbol{c}'_J\}$ and $S'_d = \{\boldsymbol{d}'_1, \ldots, \boldsymbol{d}'_J\}$). Because of the properties of GCP, the $(\boldsymbol{c}'_j, \boldsymbol{d}'_j)$ still constructs GCPs for $j = 1, \ldots, J$. For a given candidate GCP $(\boldsymbol{c}'_j, \boldsymbol{d}'_j)$, we calculate $\langle \boldsymbol{c}_i, \boldsymbol{c}'_j \odot \boldsymbol{s} \rangle$ and $\langle \boldsymbol{d}_i, \boldsymbol{d}'_j \odot \boldsymbol{s} \rangle$ for $\boldsymbol{c}_i \in C$ and $\boldsymbol{d}_i \in D$ and $s \in \{0, 1/Mu, \ldots, (Mu-1)/Mu\}$ and $u > 1$. If the results are less than or equal to β for all s, we update C and D by including the sequences in the candidate GCP to the sets.

We list the sets obtained for $\boldsymbol{c}_i$ and $\boldsymbol{d}_i$ in Table I when $\beta = 0.715$ and $u = 128$. Based on the aforementioned procedure, we could not obtain C and D when $\beta < 0.715$ for $K = 30$ and $N_{\rm sc} = 12$. However, the numerical results given in Section IV show that the maximum cross-correlation is still less than the ones for Zadoff-Chu (ZC) sequences and the sequences adopted in NR. It is also worth noting that the sets obtained for $\boldsymbol{c}_i$ and $\boldsymbol{d}_i$ are not unique and depend on the initial seed sequences.

B. Coherent Scheme

Theorem 1 allows ω_1 and ω_2 to be any unit-norm complex numbers. Hence, it indeed enables a scheme which can carry 2 QPSK symbols via sequence modulation while inheriting the low PAPR benefit of CSs. By investigating the transmitter given in Figure 2(a), it is straightforward to modulate the

[1]Contiguous allocation for random access signals typically improve the timing accuracy with a simple receiver.

Table I
THE SEQUENCES IN C AND D

i	$\boldsymbol{c}_i$	$\boldsymbol{d}_i$
1	(+,-,i,j,+,-,-,-,+,+,+,+)	(-,+,-,+,+,-,+,+,j,j,+,+)
2	(+,-,j,i,+,-,-,-,+,+,+,+)	(-,+,-,+,+,-,+,+,i,i,+,+)
3	(+,+,+,+,i,+,-,j,+,-,-,+)	(+,+,-,-,i,+,+,i,+,-,+,-)
4	(+,-,-,+,i,-,+,j,+,+,+,+)	(-,+,-,+,j,+,+,j,-,-,+,+)
5	(+,+,+,+,j,+,-,i,+,-,-,+)	(+,+,-,-j,+,+,j,+,-,+,-)
6	(+,-,-,+,j,-,+,i,+,+,+,+)	(-,+,-,+,i,+,+,i,-,-,+,+)
7	(+,+,+,+,i,-,+,j,+,-,-,+)	(+,+,-,-,i,-,-,i,+,-,+,-)
8	(+,-,-,+,i,+,-,j,+,+,+,+)	(-,+,-,+,j,-,-,j,-,-,+,+)
9	(+,+,+,+,j,-,+,i,+,-,-,+)	(+,+,-,-j,-,-,j,+,-,+,-)
10	(+,-,-,+,j,+,-,i,+,+,+,+)	(-,+,-,+,i,-,-,i,-,-,+,+)
11	(+,+,-,+,-,j,+,j,-,+,+,+)	(-,-,+,-,j,-,i,-,-,+,+,+)
12	(+,+,-,+,-,i,+,i,-,+,+,+)	(-,-,+,-,i,-,j,-,-,+,+,+)
13	(+,+,+,-,-,i,-,j,-,+,-,-)	(+,+,+,-,j,+,j,-,+,-,+,+)
14	(+,+,+,-,-,j,-,i,-,+,-,-)	(+,+,+,-,i,+,i,-,+,-,+,+)
15	(+,+,-,+,+,j,-,j,-,+,+,+)	(-,-,+,-,j,+,i,+,-,+,+,+)
16	(+,+,-,+,+,i,-,i,-,+,+,+)	(-,-,+,-,i,+,j,+,-,+,+,+)
17	(+,+,+,-,+,i,+,j,-,+,-,-)	(+,+,+,-,j,-,j,+,+,-,+,+)
18	(+,+,+,-,+,j,+,i,-,+,-,-)	(+,+,+,-,i,-,i,+,+,-,+,+)
19	(+,+,+,-,i,i,+,-,+,+,-,+)	(+,+,+,-,-,-,j,i,-,-,+,-)
20	(+,-,+,+,-,+,j,j,-,+,+,+)	(-,+,-,-,j,i,-,-,-,+,+,+)
21	(+,+,+,-,j,j,-,+,+,+,-,+)	(+,+,+,-,+,+,i,j,-,-,+,-)
22	(+,-,+,+,+,-,i,i,-,+,+,+)	(-,+,-,-,i,j,+,+,-,+,+,+)
23	(+,+,+,i,-,+,-,-,i,+,-,+)	(+,+,+,i,-,+,+,+,j,-,+,-)
24	(+,+,+,j,-,+,-,-,j,+,-,+)	(+,+,+,j,-,+,+,+,i,-,+,-)
25	(+,+,-,+,+,+,j,i,-,-,-,+)	(+,+,-,+,j,j,+,-,+,+,+,-)
26	(+,-,-,-,j,i,+,+,+,-,+,+)	(-,+,+,+,-,+,i,i,+,-,+,+)
27	(+,+,-,+,-,-,i,j,-,-,-,+)	(+,+,-,+,i,i,-,+,+,+,+,-)
28	(+,-,-,-,i,j,-,-,+,-,+,+)	(-,+,+,+,+,-,j,j,+,-,+,+)
29	(+,+,-,+,i,+,-,i,-,-,+,+)	(+,+,-,+,i,+,+,j,+,+,-,-)
30	(+,+,-,-,j,-,+,j,+,-,+,+)	(-,-,+,+,i,+,+,j,+,-,+,+)

sequences on different RBs by mapping the information bits, i.e., ACK/NACK or SR, to ω_1 and ω_2, where $\omega_1, \omega_2 \in Q_2 \triangleq \{\mathrm{e}^{\frac{\mathrm{i}\pi}{4}}, \mathrm{e}^{\frac{\mathrm{i}3\pi}{4}}, \mathrm{e}^{-\frac{\mathrm{i}\pi}{4}}, \mathrm{e}^{-\frac{\mathrm{i}3\pi}{4}}\}$. Although this approach has its own merits, the resulting scheme would require another OFDM symbol for channel estimation. On the other hand, some applications with more strict latency constraints may require a framework where a set of RSs appears in each RB for the sake of channel estimation. The question is then if there exists any set of parameters, i.e., k, l, m and initial GCPs, i.e., $(\boldsymbol{a}, \boldsymbol{b})$ of length N and $(\boldsymbol{c}, \boldsymbol{d})$ of length M such that it leads to an interlace with desired resource allocation in frequency while yielding to RSs in each RB.

To address this question, we consider a similar strategy based on Golay's interleaving method and employ Theorem 1 by choosing $k = N_{\mathrm{sc}} \times N_{\mathrm{rb}}$, $l = 2$, $m = 1$, the initial GCPs, i.e., $(\boldsymbol{a}, \boldsymbol{b})$ of length $N = N_{\mathrm{rb}}$ and $(\boldsymbol{c}, \boldsymbol{d})$ of length $M = N_{\mathrm{sc}}/2$, and the elements of $\boldsymbol{a}$, $\boldsymbol{b}$, $\boldsymbol{c}$, and $\boldsymbol{d}$ be in the set of Q_1. Similar to the non-coherent scheme, $\boldsymbol{a}$ and $\boldsymbol{b}$ act as spreading sequences for the upsampled sequences $\boldsymbol{c}$ and $\boldsymbol{d}$ with the factor of 2, respectively, as

$$p_{\boldsymbol{a}}(z^{N_{\mathrm{sc}}+N_{\mathrm{null}}})p_{\boldsymbol{c}}(z^2) = p_{\uparrow_{N_{\mathrm{sc}}+N_{\mathrm{null}}}\{\boldsymbol{a}\}*\uparrow_2\{\boldsymbol{c}\}}(z), \tag{12}$$

and

$$p_{\boldsymbol{b}}(z^{N_{\mathrm{sc}}+N_{\mathrm{null}}})p_{\boldsymbol{d}}(z^2) = p_{\uparrow_{N_{\mathrm{sc}}+N_{\mathrm{null}}}\{\boldsymbol{b}\}*\uparrow_2\{\boldsymbol{d}\}}(z). \tag{13}$$

However, unlike the non-coherent scheme, each RB is constructed based on the interleaved $\boldsymbol{c}$ and $\boldsymbol{d}$ since we choose $m = 1$ and the size of sequences $\boldsymbol{c}$ and $\boldsymbol{d}$ to be half of the RB size. Since ω_1 and ω_2 are the coefficients of (12) and (13) in (5), they are essentially multiplied with the interleaved and spread sequences $\boldsymbol{c}$ and $\boldsymbol{d}$ in each RB, as illustrated in Figure 2(b). Thus, by fixing either ω_1 and ω_2, the RSs on each RB can be obtained and the PAPR of the responding signal is still always less than or equal to 3 dB. For example, an interlace compatible with the LTE eLAA can be constructed when $k = 120$, $l = 2$, and $m = 1$ and the sequences $\boldsymbol{a}$, $\boldsymbol{b}$, $\boldsymbol{c}$, $\boldsymbol{d}$ are chosen from [19] as $\boldsymbol{a} = (+,+,+,+,+,-,+,-,-,+)$, $\boldsymbol{b} = (+,+,-,-,+,+,+,-,+,-)$, $\boldsymbol{c} = (+,+,+,\mathrm{i},-,+)$, and $\boldsymbol{d} = (+,+,\mathrm{j},-,+,-)$. Note that this scheme can support multiple access by generating orthogonal codes for $\boldsymbol{c}$ and $\boldsymbol{d}$ through (9) since the resulting sequences via (9), i.e., $(\boldsymbol{c} \odot \boldsymbol{s}, \boldsymbol{d} \odot \boldsymbol{s})$, still construct a GCP.

IV. NUMERICAL ANALYSIS

In this section, we compare the proposed schemes with other schemes in the literature numerically. For the simulations, we consider the LTE eLAA interlace parameters, i.e., $N_{\mathrm{sc}} = 12$, $N_{\mathrm{rb}} = 10$, $N_{\mathrm{null}} = 9 \times 12 = 108$ subcarriers. For the proposed non-coherent scheme, we employ the sequences given in Table I and the spreading sequences as $\boldsymbol{a} = (+,+,+,\mathrm{j},\mathrm{i})$, $\boldsymbol{b} = (+,\mathrm{i},-,+,\mathrm{j})$. For the coherent scheme, we assume that $\boldsymbol{a} = (+,+,+,+,+,-,+,-,-,+)$, $\boldsymbol{b} = (+,+,-,-,+,+,+,-,+,-)$, $\boldsymbol{c} = (+,+,+,\mathrm{i},-,+)$, and $\boldsymbol{d} = (+,+,\mathrm{j},-,+,-)$. For comparison, we consider NR sequences [15] on each RB in the interlace and three PAPR minimization methods. The first two methods rely on the optimal phase rotation with QPSK alphabet for each RB for a given sequence, i.e., PTS approach, which prioritize cubic metric (CM) and PAPR. The third approach applies a modulation operation to the sequence on each RB as a function of the occupied RB index. In other words, the sequence on kth occupied RB in the interlace is multiplied with the sequence $(\xi^{0\times k}, \xi^{1\times k}, \ldots, \xi^{(N_{\mathrm{sc}}-1)\times k})$ for $k = 0, 1, \ldots, 9$. We refer to this operation as *cycling* since the signal component located on each RB is cyclically shifted in time. For the fourth design, we generate all possible ZC sequences of length 113 (cyclically padded to 120) and select the best 30 sequences based on the PAPR of the corresponding signals after they are mapped to the interlace. For the coherent scheme, we consider NR sequences with cycling and modulate every other subcarrier to transmit ACK/NACK.

A. PAPR/CM Results

In Figure 3, the PAPR distribution for both coherent and non-coherent schemes are provided. For the alternative non-coherent schemes, the optimal spreading sequences prioritizing PAPR or CM to yield a maximum PAPR of 5.3 dB and 5.7 dB, respectively, while the ZC sequences limits the PAPR to 6 dB. The cycling reduces the maximum PAPR to 5.9 dB and 6.4 dB for non-coherent and coherent schemes, respectively. On the other hand, both of the proposed non-coherent and coherent schemes offer substantially improved PAPR results and limit the PAPR to 3 dB as it exploits CSs. The improvements in terms of PAPR are in the range of 2.7 - 3 dB and 3.4 dB as compared to alternative non-coherent and coherent schemes.

Another metric that characterizes the fluctuation of the resulting signal is the CM. We calculate the CM in dB as $CM = 20\log_{10}(\mathrm{rms}\{v_{\mathrm{norm}}^3(t)\})/1.56$, where $v_{\mathrm{norm}}(t)$ is

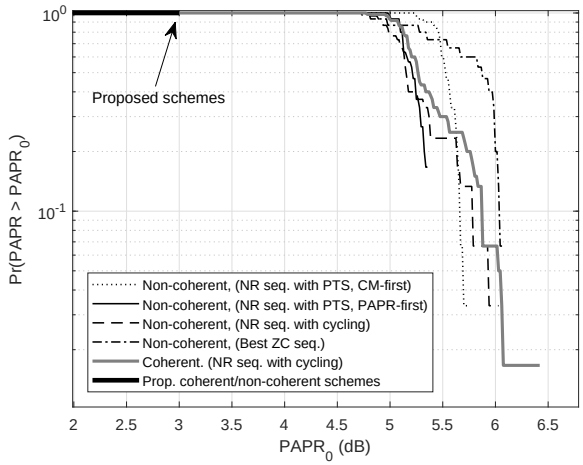


Figure 3. PAPR performance for different schemes.

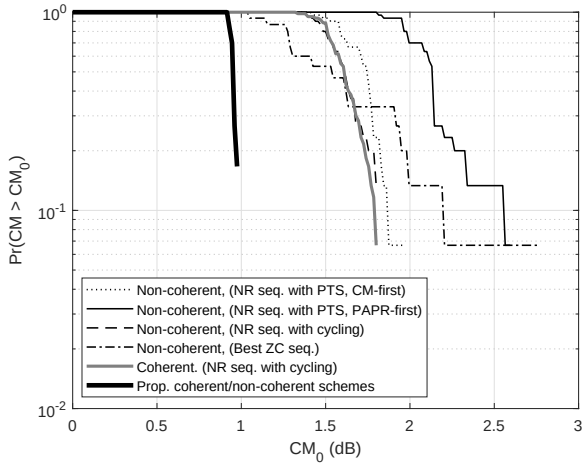


Figure 4. Cubic metric performance for different schemes.

the synthesized signal in time with the power of 1 [20]. In Figure 4, we compare CM distributions for the aforementioned schemes. Similar to the PAPR results, the proposed schemes improve the CM within the range of 0.8-1.8 dB as compared to the alternative approaches, respectively.

B. Peak Cross-correlation Performance

We evaluate the cross-correlation performance of the sequence designed for the non-coherent scheme by calculating $\rho = \max\{|\text{IDFT}\{\boldsymbol{x}_i \odot \boldsymbol{x}_j^*, N_{\text{IDFT}}\}|\}/N_{\text{sc}}$, where $\boldsymbol{x}_i$ is the ith sequence in the set, $i \neq j$ and $\text{IDFT}\{\cdot, N_{\text{IDFT}}\}$ is the unnormalized DFT operation of size N_{IDFT} [20]. To achieve a large oversampling in time, we choose $N_{\text{IDFT}} = 4096$. In Figure 5, we provide the distribution of ρ for different schemes. The ZC sequences fail as the maximum cross-correlation reaches up to 0.95 while 50 percentile performance is better than the other methods. The maximum correlation for the set of NR sequences rises to 0.8. On the other hand, the correlations for the both sets C and D are less than or equal to 0.715 as we set $\beta = 0.715$. Hence, the non-coherent scheme with C and D provides more robustness against potential inter-cell interference as compared to the one with NR sequences.

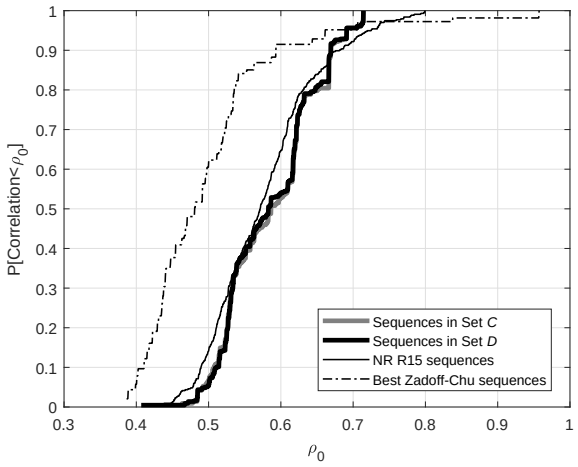


Figure 5. Peak cross-correlation distribution for the sequence sets.

C. False Alarm and Miss Detection Results

In this section, we demonstrate the impact of interlacing on the ACK-to-NACK rate and the ACK miss-detection rate for a given DTX-to-ACK probability, as compared to the single-RB approaches. The DTX-to-ACK and NACK-to-ACK rates correspond to the probability of ACK detection when there is no signal or a NACK is being transmitted, respectively. The ACK miss detection rate is the probability of not detecting ACK when ACK is actually being transmitted. For the single-RB approaches, we consider NR uplink control channel Format 0, which is a non-coherent scheme, and a coherent scheme which multiplexes RSs and data in an RB. To show the limits, we consider two extreme channel conditions where the occupied RBs in an interlace experience the same fading coefficients, i.e., flat fading, or independent-and-identically distributed (i.i.d) Rayleigh fading coefficients to model selective fading. In practice, there is always correlation between channel coefficients. However, the correlation can decrease for a large spacing between the occupied RBs in an interlace.

In the simulations, we set DTX-to-ACK probability to 1% and consider 2 receive antennas. For the baseband processing, we first detect the energy on the resources. If there is energy, we determine if it is ACK sequence or NACK sequence for non-coherent scheme. For the coherent detection, we estimate the channel and use maximum-ratio combining to combine the symbol energy on each RBs to determine if the modulation symbol is ACK or NACK. The results in Figure 6 and Figure 7 show that both non-coherent and coherent schemes have the same trends on the NACK-to-ACK and ACK miss-detection rates. In case of flat fading, the interlacing yields results worse than that of the single-RB approaches. This is expected as the baseband processing does not exploit the correlation between the channel coefficients. Otherwise, the performance of the schemes with interlace and single-RB are identical as there is no frequency diversity gain. However, when the channel is frequency-selective, the slopes of the NACK-to-ACK and ACK miss-detection rates change remarkably and the interlacing significantly improves the performance.

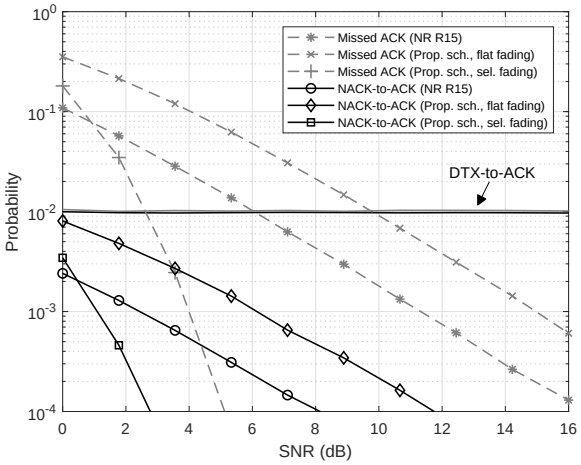


Figure 6. Receiver performance for the proposed non-coherent scheme.

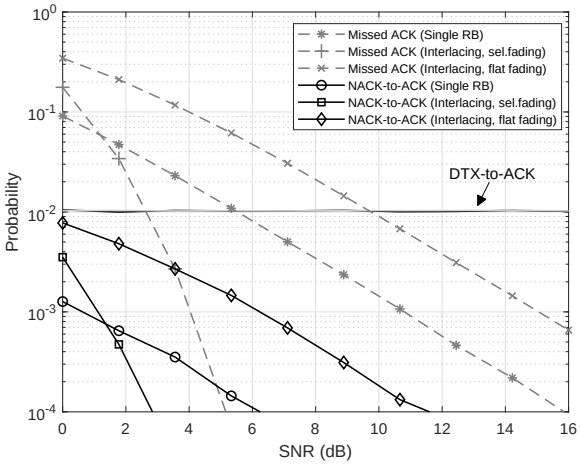


Figure 7. Receiver performance for the proposed coherent scheme.

V. Concluding Remarks

In this study, we establish a theorem which generalizes Golay's concatenation and interleaving methods to generate non-contiguous GCPs. We then discuss two schemes for uplink control channels in unlicensed spectrum by using non-contiguous GCPs. The main benefit of the proposed schemes is that they address the PAPR problem of OFDM signals while allowing a family of flexible non-contiguous resource allocations. For example, the number of null symbols between the RBs can be adjusted arbitrarily by using the same pair of spreading sequences and the sequences used in the RBs. In all cases, the PAPR of the corresponding signal is less than or equal to 3 dB. The PAPR gain is around 3 dB as compared to other schemes considered in this study.

While the first scheme can be considered as an extension of the uplink control channel Format 0 in NR for the operation in an unlicensed spectrum with non-coherent receivers, the second one achieves the same by enabling coherent detection. The first scheme separates the PAPR and inter-cell interference minimization problems. While the PAPR problem is solved by choosing the sequences for RBs as a GCP, the interference problem is addressed by designing a set of GCPs for RBs. With an algorithm which exploits the seed GCPs provided in [19], we show that there exists a set of GCPs of size 30 and length 12, which achieves a smaller maximum cross-correlation than that of NR sequences. The second scheme exploits degrees of freedom on the phases provided by Theorem 1 and leads to interleaved RSs and data symbols for each RB in an interlace.

In this study, we focus on the schemes which can carry a small amount of information, e.g., ACK/NACK or SR, with a single OFDM symbol while ensuring low PAPR and frequency diversity gain. However, there are many cases where a larger amount of information needs to be transmitted. Hence, developing more generic methods with CSs which can support more bits while achieving low PAPR and frequency diversity gain is not only theoretically interesting, but also practically appealing. We also believe that there may be other applications of non-contiguous GCPs. Further investigation of non-contiguous GCPs under different topics is highly encouraged.

References

[1] ETSI, "Harmonized EN covering the essential requirements of article 3.2 of the directive 2014/53/EU"," EN 301 893, May 2017.

[2] Y. Rahmatallah and S. Mohan, "Peak-to-average power ratio reduction in OFDM systems: A survey and taxonomy," *IEEE Commun. Surveys Tut.*, vol. 15, no. 4, pp. 1567–1592, Fourth 2013.

[3] S. H. Muller and J. B. Huber, "OFDM with reduced peak-to-average power ratio by optimum combination of partial transmit sequences," *Electronics Letters*, vol. 33, no. 5, pp. 368–369, Feb. 1997.

[4] X. Huang, J. Lu, J. Zheng, K. B. Letaief, and J. Gu, "Companding transform for reduction in peak-to-average power ratio of OFDM signals," *IEEE Trans. Wireless Commun.*, vol. 3, no. 6, pp. 2030–2039, Nov. 2004.

[5] H. Sari, G. Karam, and I. Jeanclaude, "Transmission techniques for digital terrestrial TV broadcasting," *IEEE Commun. Mag.*, vol. 33, no. 2, pp. 100–109, Feb. 1995.

[6] A. Sahin, R. Yang, F. LaSita, and R. L. Olesen, "A comparison of SC-FDE and UW DFT-s-OFDM for millimeter wave communications," in *Proc. IEEE International Communications Conference*, May 2018.

[7] A. Sahin, R. Yang, E. Bala, M. C. Beluri, and R. L. Olesen, "Flexible DFT-S-OFDM: Solutions and challenges," *IEEE Commun. Mag.*, vol. 54, no. 11, pp. 106–112, Nov. 2016.

[8] A. E. Jones, T. A. Wilkinson, and S. K. Barton, "Block coding scheme for reduction of peak to mean envelope power ratio of multicarrier transmission schemes," *Electronics Letters*, vol. 30, no. 25, pp. 2098–2099, Dec. 1994.

[9] A. E. Jones and T. A. Wilkinson, "Combined coding for error control and increased robustness to system nonlinearities in OFDM," in *IEEE Vehicular Technology Conference*, vol. 2, Apr. 1996, pp. 904–908.

[10] O. Daoud and O. Alani, "Reducing the PAPR by utilisation of the LDPC code," *IET Communications*, vol. 3, no. 4, pp. 520–529, Apr. 2009.

[11] Y. Tsai, S. Deng, K. Chen, and M. Lin, "Turbo coded OFDM for reducing PAPR and error rates," *IEEE Trans. Wireless Commun.*, vol. 7, no. 1, pp. 84–89, Jan. 2008.

[12] M. Golay, "Complementary series," *IRE Trans. Inf. Theory*, vol. 7, no. 2, pp. 82–87, Apr. 1961.

[13] J. A. Davis and J. Jedwab, "Peak-to-mean power control in OFDM, Golay complementary sequences, and Reed-Muller codes," *IEEE Trans. Inf. Theory*, vol. 45, no. 7, pp. 2397–2417, Nov. 1999.

[14] A. Sahin and R. Yang, "A generic complementary sequence encoder," *CoRR*, vol. abs/1801.09177, Oct. 2018.

[15] 3GPP, "Physical channels and modulation (Release 15)," TS 38.211 V15.1.0, Mar. 2017.

[16] S. Boyd, "Multitone signals with low crest factor," *IEEE Trans. Circuits Syst.*, vol. 33, no. 10, pp. 1018–1022, Oct. 1986.

[17] M. G. Parker, K. G. Paterson, and C. Tellambura, "Golay complementary sequences," in *Wiley Encyclopedia of Telecommunications*, 2003.

[18] J. J. Benedetto, I. Konstantinidis, and M. Rangaswamy, "Phase-coded waveforms and their design," *IEEE Signal Process. Mag.*, vol. 26, no. 1, pp. 22–31, Jan. 2009.

[19] W. H. Holzmann and H. Kharaghani, "A computer search for complex Golay sequences," *Aust. Journ. Comb.*, vol. 10, pp. 251–258, Apr. 1994.

[20] Ericsson, Nokia, Lenovo, LG, and ZTE, "WF on DMRS multi-tone evaluation methods," R1-163437, Apr. 2016.